

Quantifying net ecosystem exchange by multilevel ecophysiological and turbulent transport models

Mario Siqueira^{a,b,*}, Gabriel Katul^{a,b}, Chun-Ta Lai^c

^a *Nicholas School of Environment and Earth Sciences, Box 90328, Duke University, Durham, NC 27708-0328, USA*

^b *Department of Civil and Environmental Engineering, Duke University, Durham, NC 27708, USA*

^c *Department of Biology, University of Utah, Salt Lake City, UT, USA*

Received 30 September 2001; received in revised form 22 April 2002; accepted 23 April 2002

Abstract

To quantify the interplay between scalar sources and sinks (S_c) and net ecosystem exchange (NEE), “forward” and “inverse” approaches have been proposed. The canonical form of forward approaches is a one-dimensional ecophysiological-radiative transfer scheme coupled to turbulent transport theory. In contrast, inverse approaches strictly rely on turbulent transport theory and mean scalar concentration as their primary input to infer S_c and NEE. While the formulation of both approaches have evolved over the past decade, no systematic comparison between them was undertaken for the same data set, and over a wide range of atmospheric conditions. Our objective is to compare the predicted S_c and NEE from these two approaches with eddy-covariance measurements. The results show that the forward method outperformed all three inverse methods for unstable and neutral conditions on short time scales (~ 30 min) but yielded comparable results at longer time scales. Poor agreement was obtained under stable conditions for all models. Hence, for modeling event-based flux variations, forward models are preferred. Since the forward method requires detailed knowledge of ecophysiological, drag, radiative transfer and other canopy attributes, all of which are difficult to obtain on a routine basis, a symbiotic use of forward and inverse approaches is most advantageous.

© 2002 Elsevier Science Ltd. All rights reserved.

1. Introduction

Understanding scalar source and sink distribution (S_c) within ecosystems is critical to quantifying biosphere–atmosphere exchange, now an area of active research in hydrology, ecology, and atmospheric sciences [1–3,7,11,12,20,21,24,28,29,36,39,42]. The need to quantify S_c and its impact on land-surface fluxes at scales much larger than the “leaf” scale (e.g. canopy) requires explicit accounting of its vertical variation. This requirement lead to the development of two basic approaches. The first relies on coupling biophysical and physiological principles derived at the leaf scale with turbulent transport processes to infer S_c (e.g. CANVEG model of Baldocchi and Meyers [2]; and other similar models such as Leuning [23], and Gu et al. [12]). The second relies on the inference of S_c from turbulent transport mechanics and measured mean concentration distribution (e.g. [14,31,32,37,40]). We refer to the first

approach as “forward” because S_c is primarily inferred from knowledge about the biophysical and ecophysiological source-sink attributes. The second approach is commonly labeled as “inverse” because S_c is indirectly estimated by quantifying the variations in mean scalar concentration arising from inhomogeneity in the turbulent transport process, and attributing the remaining variations to S_c . It is clear that the fundamental assumptions underlying these two basic approaches are quite different. The forward method (FWD) requires detailed leaf-level physiological functions that are integrated to the canopy scale along the leaf area distribution, radiative and other micro-environmental vertical gradients (as well as turbulent transport mechanics). The inverse method assumes that all the information about S_c is imbedded in the measured mean concentration distribution and can be de-convolved if the turbulent mixing processes within the canopy volume are precisely quantified. While several FWD and inverse models have been proposed and field tested for some ecosystems ranging from rice fields to forests, detailed comparisons between these two approaches for the same stand has not yet been conducted.

* Corresponding author. Tel.: +919-613-8068; fax: +919-684-8741.
E-mail address: mbs4@duke.edu (M. Siqueira).

This study is the first comprehensive comparison between traditional and recent inverse models and a very detailed FWD for computing CO₂ source/sink and flux distribution within a forest canopy. The inverse models considered are the Lagrangian localized near field (LNF) method of Raupach [31,32], the Eulerian model of Katul and Albertson [14], and the recently proposed hybrid Eulerian–Lagrangian method of Siqueira et al. [37]. The FWD used is known as CANVEG after Baldocchi and Meyers [2] and is described in Lai et al. [18,19]. We emphasize that the CANVEG model was parameterized by independently collected leaf-level porometry and other ecological measurements, and was not calibrated or parameterized by canopy scale flux measurements. The results from all these methods were also compared with eddy-covariance measurements at the canopy top to assess the performance of each model. This study aims to identify the synergies, strengths and weaknesses of these approaches, and their applicability to estimate S_c from short and long-term micrometeorological variables.

2. Experimental setup

Measurements were made at the Blackwood Division of the Duke Forest near Durham, North Carolina (36°2'N, 79°8'W, elevation = 163 m). The site is a uniformly planted loblolly pine (*Pinus taeda* L.) forest that extends 300–600 m in the east–west direction and 1000 m in the north–south direction and is part of a long-term flux monitoring initiative known as AmeriFlux. The mean canopy height (h) was 14 m (± 0.5 m) at the time of the experiment. The topographic variations are small (terrain slope changes <5%) so that the influence of topography on the flow statistics can be neglected [13].

The CO₂, latent and sensible heat fluxes were measured by an eddy-covariance system comprised of a CO₂/H₂O infrared gas analyzer (Licor-6262, LI-COR, Lincoln, NE, USA), a triaxial sonic anemometer (CSAT3, Campbell Scientific, Logan, UT, USA), and a krypton hygrometer (KH₂O, Campbell Scientific). The anemometer and hygrometer were positioned 15 m above the forest floor. The hygrometer was used to assess and correct tube attenuation effects and lagged maximum cross-correlation between vertical velocity and the measured scalar concentration as discussed in Katul et al. [15,16]. Analog signals from these instruments were sampled at 10 Hz using a Campbell Scientific 21X data logger. Raw 10 Hz measurements were processed using the procedures described in Katul et al. [15,16].

Synchronous to the flux measurements, a Ta/RH probe (HMP32C, Campbell Scientific) was positioned at 15.5 m to measure the mean air temperature and relative humidity. A Fritchen-type net radiometer and a quan-

tum sensor (Q7 and LI-190SA, respectively, LI-COR) were installed to measure net radiation (R_n) and photosynthetically active radiation (PAR), respectively. All meteorological variables were sampled at 1 s and averaged every 30 min using the 21X Campbell Scientific datalogger.

A multi-port system was installed to measure the mean CO₂ and H₂O concentration inside the canopy at 10 levels (0.1, 0.75, 1.5, 3.5, 5.5, 7.5, 9.5, 11.5, 13.5 and 15.5 m). Each level was sampled for 1 min (45 s sampling and 15 s purging) at the beginning, the middle, and the end of each 30 min sampling period.

The leaf area density was measured with a LAI-2000 (LI-COR, Inc.) canopy analyzer in increments of 1 m. The leaf-level physiological parameters required by CANVEG were estimated from gas exchange measurements conducted by a portable CO₂ and H₂O infrared gas analyzer systems (CIRAS-1, PP-Systems) and is described in Ellsworth [8]. A more detailed description of the experimental setup and procedure can be found in Lai et al. [18,19].

The period considered spans from July 25 to August 13 of 1999 because of the availability of porometry and leaf area density measurements synchronous with the CO₂ concentration and flux measurements. Also, a 3-week period around July–August ensures that the measured leaf area density and other ecophysiological functions derived from porometry are static and representative of this period.

3. Theory

The fundamentals of canopy transport in the Eulerian and Lagrangian framework are briefly reviewed. The physiological functions underlying the FWD are also presented. Because the theory of both FWD and inverse models was fully described elsewhere, we only include a brief description for completeness.

3.1. Eulerian inverse model (EUL)

Applying time and horizontal averaging, the steady-state scalar conservation equation for planar homogeneous, high Reynolds and Peclet numbers flow (neglecting molecular diffusion) can be written as [10,33]

$$\frac{\partial \langle \bar{c} \rangle}{\partial t} = 0 = -\frac{\partial \langle \overline{w'c'} \rangle}{\partial z} + S_c \quad (1)$$

The overbar and $\langle \cdot \rangle$ denote time and horizontal averaging respectively [34] and primes denote fluctuations from time averages; c is the scalar concentration, w is the vertical velocity and $F_c = \langle \overline{w'c'} \rangle$ is the vertical turbulent flux.

The corresponding time and horizontally averaged conservation equation for the vertical scalar flux budget is

$$\frac{\partial \langle \overline{w'c'} \rangle}{\partial t} = 0 = -\langle \overline{w^2} \rangle \frac{\partial \langle \bar{c} \rangle}{\partial z} - \frac{\partial \langle \overline{w'w'c'} \rangle}{\partial z} - \frac{1}{\rho} \left\langle \overline{c' \frac{\partial p'}{\partial z}} \right\rangle \quad (2)$$

where ρ is the mean air density and p is the pressure. In (2), buoyancy, scalar drag, and waving source production terms were neglected. The three terms on the right-hand side of (2) represent respectively the production of turbulent flux due to interactions between the turbulent flow and the mean concentration gradient, transport of the turbulent flux, and dissipation by the pressure–scalar interaction.

The last two terms on the right-hand side of (2) are unknowns requiring closure approximations. In this study, the transport term derived by Meyers and Paw U [26] and the dissipation term modeled after Finnigan [10] were adopted. These approximations are

$$\langle \overline{w'w'c'} \rangle = \frac{\tau}{C_8} \left[-\langle \overline{w'w'w'} \rangle \frac{\partial \langle \bar{c} \rangle}{\partial z} - \langle \overline{w'c'} \rangle \frac{\partial \langle \overline{w'w'} \rangle}{\partial z} - 2\langle \overline{w'w'} \rangle \frac{\partial \langle \overline{w'c'} \rangle}{\partial z} \right] \quad (3)$$

$$\frac{1}{\rho} \left\langle \overline{c' \frac{\partial p'}{\partial z}} \right\rangle = C_4 \frac{\langle \overline{w'c'} \rangle}{\tau} \quad (4)$$

In (3) and (4), C_4 and C_8 are closure constants and τ is an Eulerian time scale given by

$$\tau = \frac{q}{\langle \varepsilon \rangle} \quad (5)$$

where $q \left(= \sqrt{\langle u_i' u_i' \rangle} \right)$ is a characteristic turbulent velocity, $\langle \varepsilon \rangle$ is the mean rate of viscous dissipation, and u_i are the velocity components in the x_1 (or x), x_2 (or y), and x_3 (or z) directions, respectively, with x_1 aligned along the mean wind direction so that $\bar{u}_2 = 0$.

Upon combining (2)–(4), a second-order ordinary differential equation (ODE) can be derived for the scalar turbulent flux [14]:

$$A_1(z) \frac{d^2 \langle \overline{w'c'} \rangle}{dz^2} + A_2(z) \frac{d \langle \overline{w'c'} \rangle}{dz} + A_3(z) \langle \overline{w'c'} \rangle = A_4(z) \quad (6)$$

where

$$A_1(z) = \frac{2\tau}{C_8} \langle \overline{w'w'} \rangle$$

$$A_2(z) = \frac{\tau}{C_8} \frac{d \langle \overline{w'w'} \rangle}{dz} + 2 \frac{d}{dz} \left(\frac{\tau}{C_8} \langle \overline{w'w'} \rangle \right)$$

$$A_3(z) = \frac{d}{dz} \left(\frac{\tau}{C_8} \frac{d \langle \overline{w'w'} \rangle}{dz} \right) - C_4 \frac{1}{\tau}$$

$$A_4(z) = \langle \overline{w'w'} \rangle \frac{d \langle \bar{c} \rangle}{dz} - \frac{d}{dz} \left(\frac{\tau}{C_8} \langle \overline{w'w'w'} \rangle \right) \frac{d \langle \bar{c} \rangle}{dz} - \left(\frac{\tau}{C_8} \langle \overline{w'w'w'} \rangle \right) \frac{d^2 \langle \bar{c} \rangle}{dz^2}$$

The measured mean concentration profile is used only to calculate its gradient and curvature in $A_4(z)$, the non-homogeneous term of the ODE. The flow statistics $\langle \overline{w'w'} \rangle$, $\langle \overline{w'w'w'} \rangle$ and τ can be estimated from second-order closure principles such as the momentum transport model proposed by Wilson and Shaw [41]. Finally (6) can be numerically solved for $\langle \overline{w'c'} \rangle$, which upon differentiation with respect to z , results in S_c . This S_c can now be compared with estimates from the CANVEG (or FWD) model. The boundary conditions for (6) are

$$\begin{aligned} z \geq h: \quad \langle \overline{w'c'} \rangle &= \frac{A_4(h)}{A_3(h)} \\ z = 0: \quad \frac{d \langle \overline{w'c'} \rangle}{dz} &= 0 \end{aligned} \quad (7)$$

where h is the canopy height.

Eqs. (6) and (7) constitute the EUL of Katul and Albertson [14]. The constants used in the present calculations were $C_4 = 2.5$ and $C_8 = 3.0$ as discussed in Siqueira et al. [37].

4. Hybrid Eulerian–Lagrangian method (HEL)

The HEL approach adopts the second-order closure model described above to estimate the elements of the dispersion matrix [31] and computes S_c from a regression algorithm. The second-order ODE describing the concentration profile from a prescribed unit source (and hence the flux as in (1)) can be derived from (2)–(4) and is given by

$$B_1(z) \frac{d^2 \langle \bar{c} \rangle}{dz^2} + B_2(z) \frac{d \langle \bar{c} \rangle}{dz} = B_3(z) \quad (8)$$

where

$$B_1(z) = \frac{\tau}{C_8} \langle \overline{w'w'w'} \rangle$$

$$B_2(z) = -\langle \overline{w'w'} \rangle + \frac{d}{dz} \left(\frac{\tau}{C_8} \langle \overline{w'w'w'} \rangle \right)$$

$$\begin{aligned} B_3(z) = & -\frac{d}{dz} \left[\frac{\tau}{C_8} \left(\langle \overline{w'c'} \rangle \frac{d \langle \overline{w'w'} \rangle}{dz} + 2 \langle \overline{w'w'} \rangle \frac{d \langle \overline{w'c'} \rangle}{dz} \right) \right] \\ & + C_4 \frac{\langle \overline{w'c'} \rangle}{\tau} \end{aligned}$$

In (8), $\langle \overline{w'c'} \rangle$ is the turbulent flux profile calculated by integrating the unit source placed at one layer via (1). That is, the elements of D_{ij} are computed by (1) positioning a unit source at a layer corresponding to node j ; (2) integrating this source profile to obtain the $\langle \overline{w'c'} \rangle$ profile; and (3) solving the ODE in (8) for the concentration at all i nodes ($i = 1, \dots, n$) resulting from the source placed at node j . This procedure is repeated for $j = 1, \dots, m$ to obtain all the elements of the D_{ij} matrix.

5. Localized near field (LNF) theory

The LNF theory calculates the mean scalar concentration relative to a reference value $\langle \bar{c} \rangle_R$ measured above the canopy at some reference height (z_R ; $z_R > h$) by super-imposing near field (C_n) and far field (C_f) contributions:

$$\langle \bar{c} \rangle - \langle \bar{c} \rangle_R = C_n + C_f \quad (9)$$

As shown in Raupach [31,32], the near field contribution is computed via a kernel function:

$$C_n(z) = \int_0^\infty \frac{S_c(z_0)}{\sigma_w(z_0)} \left[k_n \left(\frac{z - z_0}{\sigma_w(z_0) T_L(z_0)} \right) + k_n \left(\frac{z + z_0}{\sigma_w(z_0) T_L(z_0)} \right) \right] dz_0 \quad (10)$$

where $\sigma_w = (\sqrt{\overline{w'w'}})$ is the standard deviation of vertical velocity and T_L is the Lagrangian integral time scale. An analytical approximation for the kernel function k_n was derived by Raupach [31] and is given by

$$k_n(\xi) = -0.39894 \ln(1 - e^{-|\xi|}) - 0.15623 e^{-|\xi|} \quad (11)$$

The far field contribution is calculated using the result from near field and a gradient–diffusion relationship such that

$$C_f(z) = \langle \bar{c} \rangle_R - C_n(z_R) + \int_z^{z_R} \frac{\overline{w'c'}}{K_f(z)} dz \quad (12)$$

The far field diffusivity K_f can be approximated by

$$K_f(z) = \sigma_w^2(z) T_L(z) \quad (13)$$

Raupach [31] suggested that T_L might be of the same order as the canopy time scale h/u_* (also discussed in Raupach et al. [30]) such that

$$\frac{T_L(z) u_*}{h} = \beta \quad (14)$$

where u_* is the friction velocity and β is a constant (here $\beta = 0.1$ was used).

The dispersion matrix is computed from

$$D_{ij} = \frac{\langle \bar{c} \rangle_i - \langle \bar{c} \rangle_R}{s \Delta z_j} \quad (15)$$

A similar procedure as described for HEL could be applied with the dispersion matrix calculated by (15). A more detailed description of the inverse models can be found in Siqueira et al. [37].

The implementation of LNF here departs from Raupach's [31,32] original formulation to include a smoothing penalty function, known as weighted measure of length procedure [25]. This revision was shown to greatly improve the accuracy of LNF [37].

5.1. CANVEG FWD

The CANVEG approach of Baldocchi and Meyers [2] couples conservation equations for mean scalar mass (mainly CO₂ and water vapor) and heat, as given by (1), a Lagrangian turbulent dispersion algorithm, energy and radiation conservation, and biophysical and physiological mechanisms responsible for stomatal opening and carbon assimilation. In (1), $\langle \bar{c} \rangle$ is the mean scalar concentration or temperature (i.e. H₂O, CO₂, and temperature T), $\overline{w'c'}$ is the mean vertical flux of a scalar entity c (e.g. F_{CO_2} , F_{H_2O} , and F_T are CO₂, H₂O, and sensible heat turbulent fluxes respectively), and S_c is the mean vegetation source strength above the forest floor. Using the concept of dispersion matrix as in HEL or LNF, a prognostic equation establishes the interdependency between source and concentrations:

$$\langle \bar{c} \rangle - \langle \bar{c} \rangle_R = \sum_{j=1}^N S_{cj} D_{ij} \Delta z_j \quad (16)$$

where i and j are the indices for concentration and source strength location respectively, Δz_j is the discrete layer thickness within the canopy, N is number of layers within the canopy volume and subscript R refers to a reference height. In this implementation the D_{ij} matrix is calculated by following the trajectory of an ensemble of fluid parcels, using the random walk algorithm of Thompson [38], released uniformly from a unit source placed at each j th layer. Like EUL and HEL, Wilson and Shaw's [41] second-order closure model provides the required velocity statistics for the calculation of scalar dispersion. We emphasize that both forward and inverse calculations adopted the same flow statistics, and hence, differences between them cannot be attributed to the specification of the flow field.

An additional equation is derived from physiological controls on S_c :

$$S_c(z) = -\rho a(z) \frac{\langle \bar{c} \rangle(z) - \bar{c}_{ic}(z)}{r_b(z) + r_s(z)} \quad (17)$$

where, $a(z)$ is the plant area density, \bar{c}_{ic} is the mean intercellular scalar concentration, $r_b(z)$ is the boundary layer resistance, and $r_s(z)$ is the stomatal resistance. Eqs. (16) and (17) permit a complete mathematical description of $\langle \bar{c} \rangle$, F_c and S_c if \bar{c}_{ic} , r_s , and r_b are known or parameterized.

The estimation of r_b is based on flat plate theory [2,35] and is given by

$$r_b = \frac{l_d}{d_m Sh} \quad (18)$$

where l_d is the characteristic leaf length scale, d_m is the molecular diffusivity of a scalar entity, and Sh is the Sherwood number, which can be determined from the mean longitudinal velocity inside the canopy.

The stomatal conductance G_s ($= r_s^{-1}$) is computed by linking G_s to leaf photosynthesis (A_n), relative humidity (rh) and CO_2 concentration at the leaf surface (\bar{c}_s), as described by Ball et al. [4] and Collatz et al. [6], and is given by

$$G_s = m \frac{A_n rh}{\bar{c}_s} + b \quad (19)$$

where m and b are empirical parameters that vary with vegetation type (but can be independently determined from porometric measurements). According to Farquhar et al. [9] photosynthesis model, A_n is given by

$$A_n \approx \min \left\{ \begin{matrix} J_E \\ J_C \\ J_S \end{matrix} \right\} - R_d \quad (20)$$

where J_E and J_C are the assimilation rates restricted by either electron transport through the photosystem or ribulose biphosphate (R_uBP) carboxylase (Rubisco), respectively, and R_d is the respiration rate during daytime but in the absence of photorespiration. The formulation and parameterization of J_E , J_C and R_d as a function of PAR, the intercellular CO_2 concentration (c_i), and surface temperature (T_s) are presented in Lai et al. [19]. Note that (19) and (20) require A_n , rh and T_s within the canopy, hence, all three scalars (H_2O , CO_2 and T) must be simultaneously considered in (1), (16) and (17) (i.e. 9 equations).

An energy budget is employed at the leaf surface for each level within the canopy to compute both mean leaf temperature (T_s) and absorbed radiation. These parameters are necessary to calculate c_i for the model of Farquhar et al. [9] and to account for the dependency of leaf assimilation rate on T_s .

The extra-terrestrial radiation was decomposed into solar radiation and thermal radiation. The solar radiation was further divided into direct beam and diffuse radiation [5,27]. After subtracting the reflected quantities for PAR and near-infrared radiation (NIR) by the canopy surface, the remaining radiation is transmitted through canopy volume. The light transmission through the canopy is computed for sunlit and shaded portions separately to estimate PAR and NIR irradiance absorbed at each canopy level using the model of Campbell and Norman [5]. See [19] for the details on the calculation of canopy light attenuation.

6. Results and discussion

Comparisons between computed fluxes and sources by the three inverse methods and one FWD are conducted. For the three inverse methods, mean CO_2 concentration profiles within and above the canopy as well as the friction velocity (u_*) above the canopy are used as input. For the FWD, the forcing variables include

measured incident radiation, mean streamwise velocity component, mean air temperature, mean CO_2 and water vapor concentrations above the canopy. The physiological and canopy attributes include leaf area density distribution along with the parameters of the Collatz et al. [6] model as described in Lai et al. [18,19]. Comparisons between the modeled fluxes and eddy-covariance measurements at the canopy top are also discussed.

The grid arrangements for each model were as follows: for EUL the calculation domain was discretized into a 165 node uniform mesh; for HEL and LNF the canopy was divided into seven layers. For FWD the canopy was divided into 14 evenly spaced layers. Note that the number of layers for HEL and LNF is less than that for FWD. The reason is that it is desirable to have redundant data points (when possible) to decrease the model sensitivity to concentration measurement errors. Sensitivity to the choice of the grid spacing is described elsewhere [37].

6.1. Generation of the flow statistics inside the canopy

The implementation of EUL and HEL requires the standard deviation of vertical velocity, σ_w , (also needed by LNF and FWD), relaxation time scale, and the third moment of vertical velocity. The second-order closure model of Wilson and Shaw [41], using the measured leaf area density shown in Fig. 1b, was used to generate these velocity statistics. Siqueira et al. [37] compared the velocity statistics measured and calculated with the model of Wilson and Shaw [41] for the same stand but for a different period. They concluded that the performance of this closure model is sufficiently adequate for conducting scalar transport calculations. Fig. 1a shows the

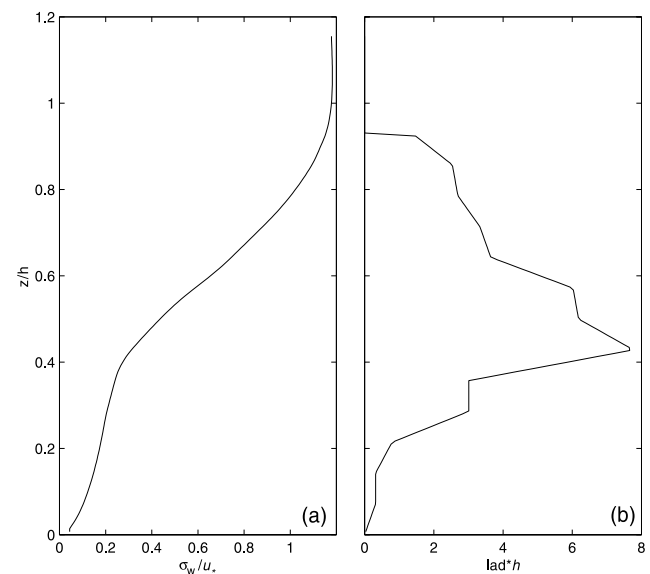


Fig. 1. (a) Modeled standard deviation of vertical velocity normalized by u_* above the canopy. (b) Measured leaf area density.

calculated σ_w normalized by u_* , which is the critical velocity statistic in all models. As expected, the calculated σ_w is attenuated in the deeper layers of the canopy but sharply increases after the leaf area density peaks.

To account for atmospheric stability on scalar transport, corrections to the flow statistics and relaxation time scale, τ , and Lagrangian integral time scale, T_L , for $z/L > 0$ at the canopy top (where L is Obukhov length) were conducted as described by Lai et al. [17].

6.2. Comparison with eddy-covariance flux measurements

Fig. 2 shows the 1 to 1 comparisons between the models and eddy-covariance measurements for various stability conditions. Table 1 presents the statistical parameters of this comparison. It is clear that the FWD outperforms the inverse models for all stability conditions (see Table 1). In particular, under near-neutral stability condition, FWD agrees better with the measurements when compared to the three inverse models.

Under unstable conditions the agreement degraded for all methods yet the FWD still produced superior results. Despite the corrections applied to the relaxation time scale, τ , and Lagrangian integral time scale, T_L , for $z/L > 0$ (where L is Obukhov length), poor agreement is still observed under stable conditions for all four methods. None of them considered the local stability effects in their formulation. It is clear that corrections applied to the time scale alone are not sufficient to improve the model predictive skills.

A comparison between measured and modeled CO_2 fluxes under neutral conditions, bin-averaged by time of the day is shown in Fig. 3. All models captured the canonical form of CO_2 uptake during photosynthesis periods and CO_2 release during nighttime respiration periods. The three inverse models produced more erratic flux distribution when compared to the FWD model. This is of no surprise given their hypersensitivity to unavoidable measurement errors in the mean concentration. This problem could be minimized with longer ensemble averaging periods. The FWD, being driven by

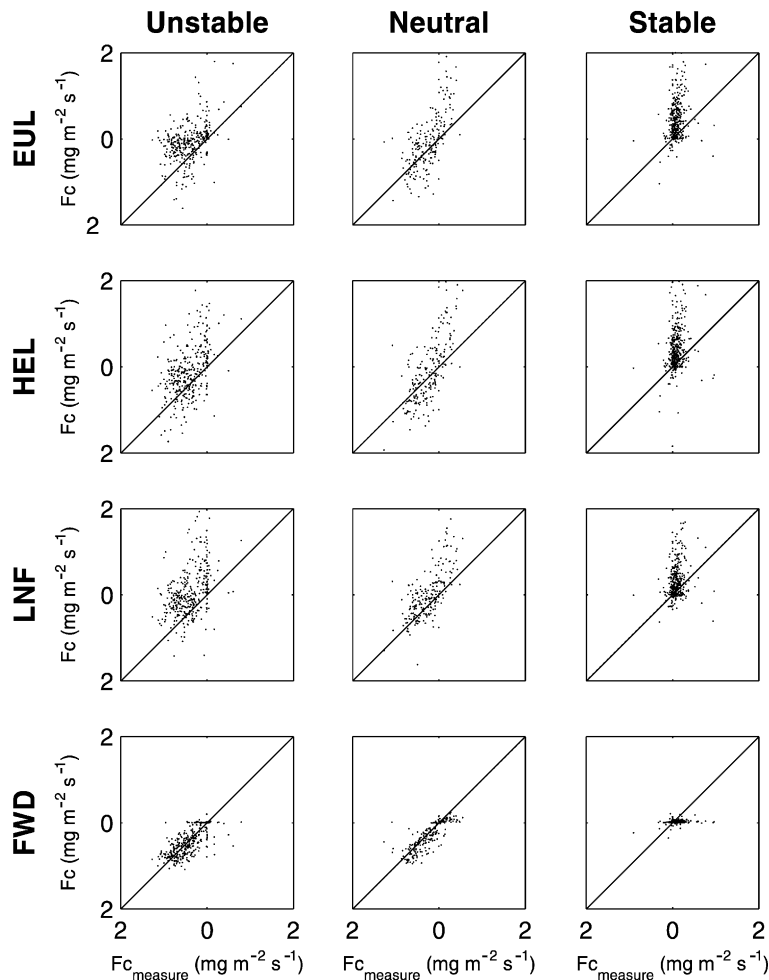


Fig. 2. A 1 to 1 comparisons for CO_2 flux at the canopy top for the four different models. The results are divided by atmospheric stability classes computed from measurements above the canopy.

Table 1

Comparison between measured [F_c (ec)] and modeled [F_c (model)] CO_2 fluxes ($mg\ m^{-2}\ s^{-1}$) above the canopy for each model and atmospheric stability condition. The regression model is F_c (model) = Slope F_c (ec) + Intercept. The correlation coefficient (R) and the root-mean-squared error (RMSE, $mg\ m^{-2}\ s^{-1}$) are shown. N is the number of profiles for each stability condition

		EUL	HEL	LNF	FWD
Unstable	N	335	335	335	335
	Slope	0.37	0.65	0.74	0.46
	Intercept ($mg\ m^{-2}\ s^{-1}$)	0.06	0.18	0.37	-0.24
	RMSE ($mg\ m^{-2}\ s^{-1}$)	0.62	0.77	0.90	0.33
	R	0.29	0.35	0.36	0.58
Neutral	N	210	210	210	210
	Slope	1.45	1.55	1.30	0.76
	Intercept ($mg\ m^{-2}\ s^{-1}$)	0.38	0.31	0.33	-0.13
	RMSE ($mg\ m^{-2}\ s^{-1}$)	0.72	0.71	0.66	0.22
	R	0.61	0.62	0.59	0.81
Stable	N	352	352	352	352
	Slope	1.01	0.87	0.74	0.07
	Intercept ($mg\ m^{-2}\ s^{-1}$)	0.41	0.36	0.29	0.01
	RMSE ($mg\ m^{-2}\ s^{-1}$)	0.68	0.68	0.55	0.16
	R	0.27	0.22	0.23	0.27

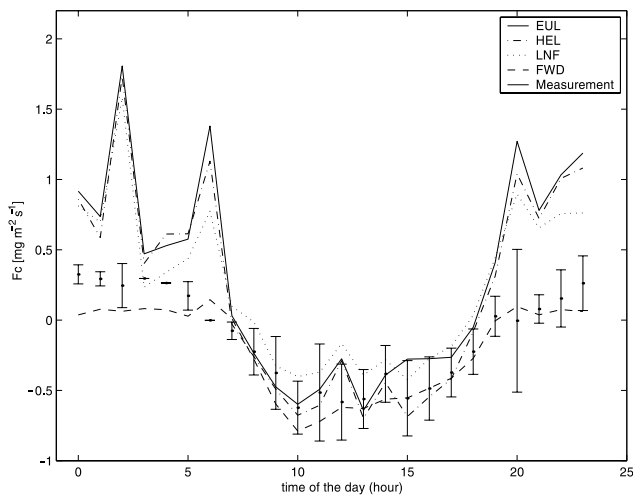


Fig. 3. Comparison between measured (dots) and modeled (lines) ensemble averaged temporal variation of CO_2 fluxes above the canopy. For reference, one standard deviation of the binned F_c (measured) is also shown.

gradually varying forcing variables (e.g. incident radiation) resulted in a smooth solution for fluxes. However, the model overestimated the negative CO_2 flux especially in the morning (between 8:00 and 10:00). When the respiration dominates the CO_2 exchange processes, all models fail to reproduce well the positive CO_2 flux. The inverse models highly overestimate the respiration fluxes due to the large concentration gradient during nighttime resulting from CO_2 build up in the lower canopy layers (see Fig. 6a) and is interpreted as a source term rather than storage flux. FWD underestimated the CO_2 flux

possibly an indication that the model underestimates nighttime plant respiration.

6.3. Comparisons of source and flux distributions between FWD and inverse models

Having discussed the limitation of these models in reproducing the fluxes above the canopy, we proceed to compare their estimated vertical flux and S_c distributions. Fig. 4a shows an ensemble contour map of the CO_2 flux distribution as a function of time of the day and depth, and Fig. 4b the CO_2 flux profiles averaged around noon (11:00–13:00). All models produced similar patterns of CO_2 uptake when photosynthesis dominated. The models predicted a maximum CO_2 flux between 10:00 and 12:00. After 12:00, FWD estimated a linear decrease in the CO_2 uptake while the inverse models presented a secondary maximum around 16:00 (see Figs. 3 and 4a).

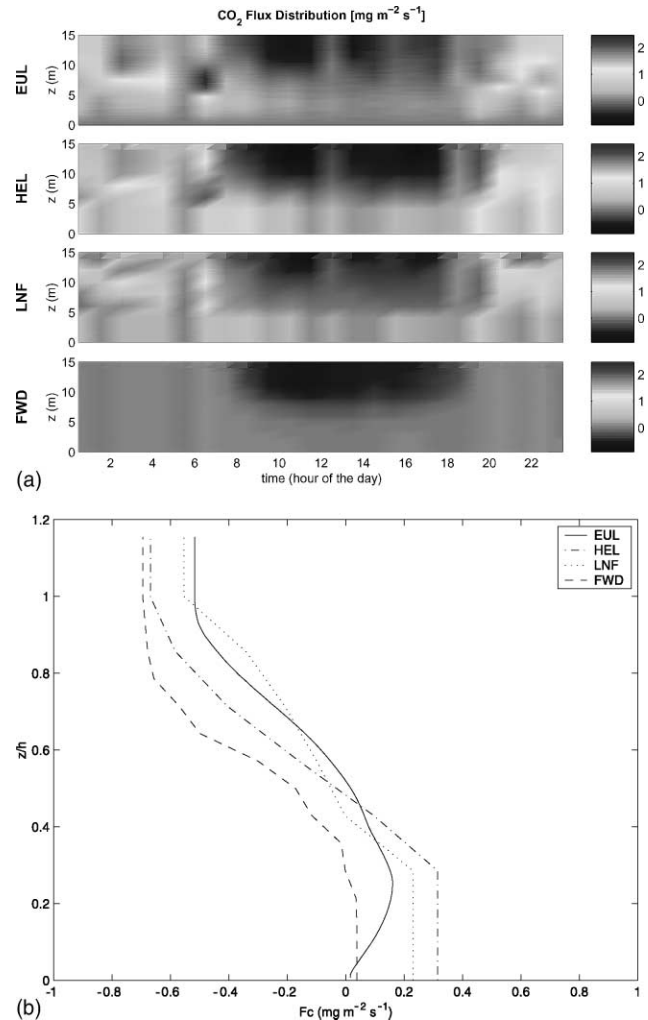


Fig. 4. (a) Contour plot of ensemble averaged CO_2 flux distribution inside the canopy as a function of height and time for the four methods considered here. (b) Vertical profiles of CO_2 fluxes averaged for period 11:00–13:00.

Similar to the results presented by Leuning [22] for a rice canopy, the inverse models estimated a higher ground CO₂ flux when compared to FWD (Fig. 4b). This discrepancy could be attributed to uncertainties in the specification of the turbulent time scale in the lower layers of the canopy. EUL showed a near-zero ground flux due to the fact that the velocity statistics are very small in the deeper canopy layers. However, just above the ground, the flux increases to a level similar to HEL and LNF. Since the leaf area density is small in this region, this higher flux could well be interpreted as a ground flux for this model.

In contrast to flux distribution, discrepancies between calculated source strength distribution by each model are more pronounced (Fig. 5a). The FWD model shows a smooth distribution of CO₂ sink during daylight period as a result of the integrated light attenuation (i.e.

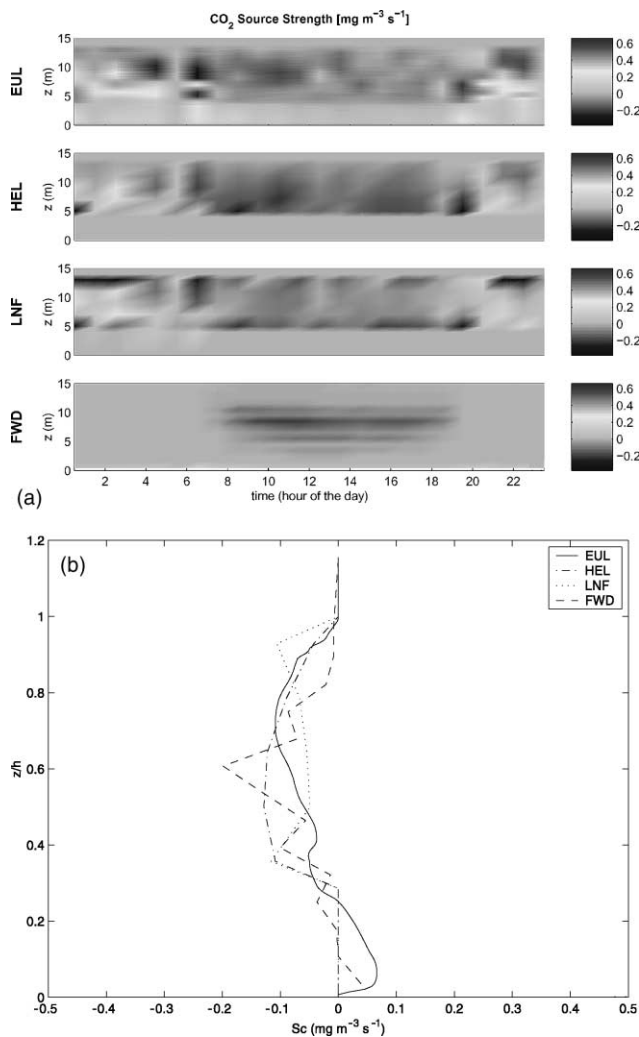


Fig. 5. (a) Contour plot of ensemble averaged CO₂ source/sink distribution inside the canopy as a function of height and time of day for all four methods. (b) Vertical profiles of CO₂ sources/sinks averaged for period 11:00–13:00 are shown as representatives for maximum canopy CO₂ net uptake.

averaging over the irregularity in leaf area density). During nighttime, the FWD estimated little plant respiration. The inverse models predicted rather erratic distribution clearly highlighting the low “signal to noise” ratio in inferring sources from such concentration measurements. During daylight hours, the models predicted the same order of magnitude source strength with HEL and FWD source distributions being most consistent. For nighttime, the inverse models generated unrealistic high source strength. Fig. 5b reveal that, around noon, FWD and HEL predicted a maximum CO₂ sink strength at mid canopy ($0.4 < z/h < 0.6$) which is co-located with the region of maximum leaf area density while EUL and LNF estimated the maximum closer to the canopy top (see Fig. 5b). LNF also predicted a local maximum at the bottom layer of the canopy ($z/h = 0.3$).

Fig. 6a shows the mean CO₂ concentration distributions measured (and used by the inverse models) and

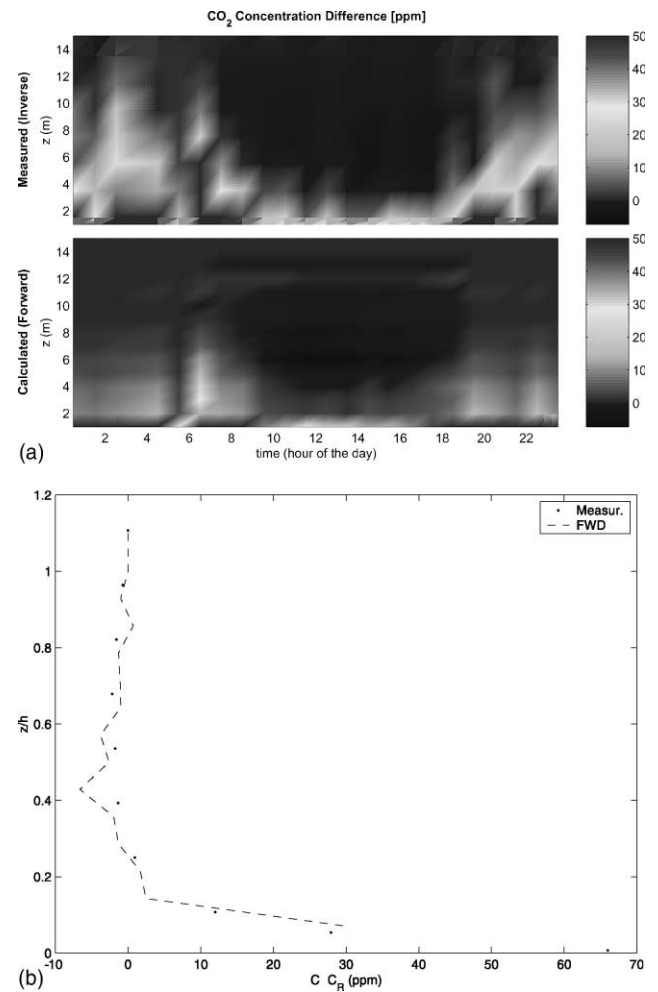


Fig. 6. (a) Contour plot of ensemble averaged CO₂ concentration distribution inside the canopy as a function of height and time. Top panel refers to measured concentration and bottom panel calculated with FWD. (b) Vertical profiles of CO₂ concentration measured and modeled by FWD averaged for period 11:00–13:00 are also shown.

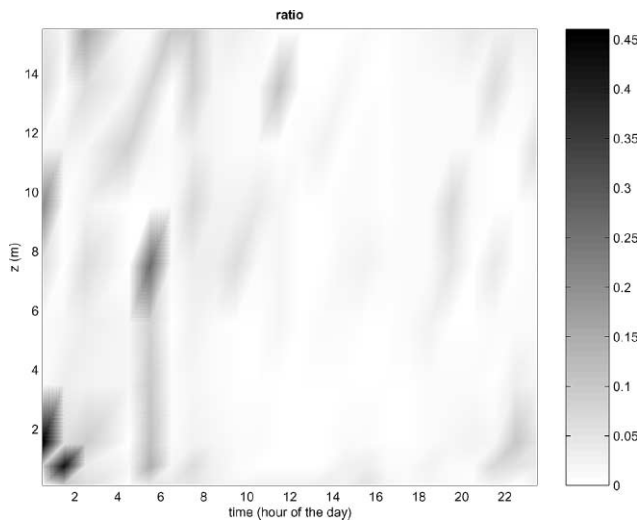


Fig. 7. Contour plot of ensemble-averaged measured $d\text{CO}_2/dt$ normalized by a reference value of $0.1 \text{ mg m}^{-3} \text{ s}^{-1}$ as a representative order of magnitude of CO_2 source over the active region of the forest.

calculated by FWD. The FWD predicted the lowest CO_2 value around noon while the lowest measured CO_2 occurred later in the day. FWD was able to reproduce the overall mean CO_2 concentration depletion inside the canopy even though the measured CO_2 is apparently more well mixed (see also Fig. 6b). During nighttime, the FWD failed to properly reproduce the CO_2 build up in the deeper layers of the canopy. We emphasize that none of the inverse models considered the storage terms in their formulations.

To assess how and when this assumption leads to potentially large errors, we conducted a study on the relative importance of the storage term. Fig. 7 shows a distribution of normalized time derivative of CO_2 (i.e. the storage term inferred from the measured concentration). A reference source of $0.1 \text{ mg m}^{-3} \text{ s}^{-1}$, representative of the mean CO_2 sink magnitude across the most active region of the canopy is chosen as a normalizing variable. It is clear that storage effects are significant during nighttime and early morning, which corresponds to the periods where all models have the poorest performance. Hence, some of the departure from calculated and measured values could be attributed to the steady-state assumption inherent to all the methods.

7. Conclusions

A comparison between three inverse models and one FWD to estimate CO_2 fluxes and source/sink strengths within a pine canopy was conducted. From this analysis it was shown that

- The FWD better reproduces the statistics of the CO_2 flux at the canopy top for all stability conditions

when compared to the three inverse methods. As expected, all models provided best results for near-neutral atmospheric stability condition. Very poor agreement was noted for stable condition.

- On average, the models exhibit a similar distribution of CO_2 fluxes inside the canopy during daylight period, but the inverse models estimated much higher CO_2 ground flux during nighttime.
- Discrepancies between models are more apparent in the source distribution when compared to the flux. All in all, HEL and FWD provided the most consistent CO_2 uptake patterns during net photosynthesis periods. None of the models reproduced well nighttime respiration.
- The CO_2 storage, not considered in any method thus far, is shown to be important during nighttime and early morning hours.

These findings suggest that FWDs are better suited for reproducing the 30-min flux variation than inverse models at the expense of detailed physiological parameterization. At longer time scales (i.e. weeks), both FWD and inverse models provided comparable results, at least in an ensemble average sense. Given the large number of parameters needed for the FWD and given the difficulty in estimating S_c in forested systems at different time scales, a combination of these different approaches in a symbiotic methodology is suggested.

Acknowledgements

The first author thanks the ‘‘Conselho Nacional de Desenvolvimento Científico e Tecnológico (CNPq)’’ of Brazil for their support. Additional support was provided by the National Science Foundation through their WEAVE program (NSF-EAR) and Directorate of Mathematical Statistics (NSF-DMS), the Department of Energy (DOE) through the TCP and FACE-FACTS project, and through the National Institute of Global Environmental Change (NIGEC) through the Southeast Regional Center at the University of Alabama, Tuscaloosa. Finally, we thank Judd Edburn and the Duke Forest staff for their overall assistance during many of these field experiments.

References

- [1] Anthoni PM, Law BE, Unsworth MH. Carbon and water vapor exchange of an open-canopied ponderosa pine ecosystem. *Agric Forest Meteorol* 1999;95:151–68.
- [2] Baldocchi D, Meyers T. On the eco-physiological and biogeochemical theory to evaluate carbon dioxide, water vapor and trace gas fluxes over vegetation: a perspective. *Agric Forest Meteorol* 1998;90:1–25.
- [3] Baldocchi D, Harley PC. Scaling carbon dioxide and water vapor exchange from leaf to canopy in a deciduous forest. II.

- Model testing and application. *Plant Cell Environ* 1995;18:1157–73.
- [4] Ball JT, Woodrow IE, Berry JA. A model predicting stomatal conductance and its contribution to the control of photosynthesis under different environmental conditions. In: Biggens J, editor. *Progress in photosynthesis research*. The Netherlands: Martinus Nijhoff Publishers; 1987. p. 221–4.
- [5] Campbell GS, Norman JM. *An introduction to environmental biophysics*. New York: Springer-Verlag; 1998.
- [6] Collatz GJ, Ball JT, Grivet C, Berry JA. Physiological and environmental regulation of stomatal conductance, photosynthesis and transpiration: a model that includes a laminar boundary layer. *Agric Forest Meteorol* 1991;54:107–36.
- [7] Culf AD, Fisch G, Malhi Y, Nobre CA. The influence of the atmospheric boundary layer on carbon dioxide concentrations over a tropical forest. *Agric Forest Meteorol* 1997;85:149–58.
- [8] Ellsworth DS. Seasonal CO₂ assimilation and stomatal limitations in a *Pinus Taeda* canopy. *Tree Physiol* 2000;20:435–45.
- [9] Farquhar GD, Von Caemmerer S, Berry JA. A biochemical model of photosynthetic CO₂ assimilation in leaves of C₃ species. *Planta* 1980;149:78–90.
- [10] Finnigan JJ. Turbulent transport in plant canopies. In: Hutchinson BA, Hicks BB, editors. *The forest–atmosphere interactions*. D. Norwell, Mass: Reidel; 1985. p. 443–80.
- [11] Gao W, Wesely ML, Doskey PV. Numerical modeling of the turbulent diffusion and chemistry of NO_x, O₃, isoprene, and other reactive trace gases in and above a forest canopy. *J Geophys Res* 1993;98:18,339–53.
- [12] Gu LH, Shugart HH, Fuentes JD, Black TA, Shewchuk SR. Micrometeorology, biophysical exchange and NEE decomposition in a two-story boreal forest—development and test of an integrated model. *Agric Forest Meteorol* 1999;94:123–48.
- [13] Kaimal JC, Finnigan JJ. In: *Atmospheric boundary layer flows their structure and measurement*. Oxford: Oxford Press; 1994. 289 pp.
- [14] Katul GG, Albertson JD. Modeling CO₂ sources, sinks and fluxes within a forest canopy. *J Geophys Res* 1999;104:6081–91.
- [15] Katul GG, Oren R, Ellsworth D, Hsieh CI, Phillips N, Lewin K. A Lagrangian dispersion model for predicting CO₂ sources, sinks, and fluxes in a uniform loblolly pine (*Pinus taeda* L.) stand. *J Geophys Res* 1997;102:9309–21.
- [16] Katul GG, Hsieh CI, Kuhn G, Ellsworth D, Nie D. Turbulent eddy motion at the forest–atmosphere interface. *J Geophys Res* 1997;102:13,409–21.
- [17] Lai CT, Katul G, Butnor J, Ellsworth D, Orem R. Modeling nighttime ecosystem respiration by a constrained source optimization method. *Global Change Biol* 2002;8(2):124–41.
- [18] Lai CT, Katul G, Oren R, Ellsworth D, Schafer K. Modeling CO₂ and water vapor turbulent flux distributions within a forest canopy. *J Geophys Res* 2000;105(D21):26,333–51.
- [19] Lai CT, Katul GG, Ellsworth D, Oren R. Modeling vegetation–atmosphere CO₂ exchange by a coupled Eulerian–Lagrangian approach. *Bound-Lay Meteorol* 2000;95:91–122.
- [20] Law BE, Baldocchi D, Anthoni PM. Below-canopy and soil CO₂ fluxes in a ponderosa pine forest. *Agric Forest Meteorol* 1999;94:171–88.
- [21] Lee XH. On micrometeorological observations of the surface–air exchange over tall vegetation. *Agric Forest Meteorol* 1998;91:39–49.
- [22] Leuning R. Estimation of scalar source/sink distributions in plant canopies using Lagrangian dispersion analysis: corrections for atmospheric stability and comparison with a multilayer canopy model. *Bound-Lay Meteorol* 2000;96(1–2):293–314.
- [23] Leuning R. A critical appraisal of a combined stomatal-photosynthesis model for C₃ plants. *Plant Cell Environ* 1995;18:339–57.
- [24] Malhi Y, Nobre AD, Grace JG, Kruijt B, Pereira MGP, Culf A, et al. Carbon dioxide transfer over a Central Amazonian rain forest. *J Geophys Res* 1998;103:31,593–612.
- [25] Menke W. Geophysical data analysis: discrete inverse theory. In: *International geophysical series*. 45 rev. ed. New York: Academic Press; 1989.
- [26] Meyers T, Paw U KT. Modeling the plant canopy micrometeorology with higher-order closure principles. *Agric Forest Meteorol* 1987;41:143–63.
- [27] Monteith JL, Unsworth MH. *Principles of environmental physics*. London: Edward Arnold; 1990. p. 58–259.
- [28] Potosnak M, Wofsy SC, Denning AS, Conway TJ, Munger JW, Barnes DH. Influence of biotic exchange and combustion sources on atmospheric CO₂ concentrations in New England from observations at a forest flux tower. *J Geophys Res* 1999;104:9561–9.
- [29] Rannik U. On the surface similarity at a complex forest site. *J Geophys Res* 1998;103:8,685–97.
- [30] Raupach MR, Finnigan JJ, Brunet Y. Coherent eddies and turbulence in vegetation canopies: the mixing-layer analogy. *Bound-Lay Meteorol* 1996;78:351–82.
- [31] Raupach MR. Applying Lagrangian fluid mechanics to infer scalar source distributions from concentration profiles in plant canopies. *Agric Forest Meteorol* 1989;47:85–108.
- [32] Raupach MR. A practical Lagrangian method for relating scalar concentrations to source distributions in vegetation canopies. *QJR Meteorol Soc* 1989;115:609–32.
- [33] Raupach MR. Canopy transport processes. In: Steffen WL, Denmead OT, editors. *Flow and transport in the natural environment*. New York: Springer-Verlag; 1988. p. 95–127.
- [34] Raupach MR, Shaw RH. Averaging procedures for flow within vegetation canopies. *Bound-Lay Meteorol* 1982;22:79–90.
- [35] Schuepp PH. Tansley review No. 59: leaf boundary layers. *New Phytol* 1993;125:477–507.
- [36] Simpson IJ, Thurtell GW, Neumann HH, Hartog G, Edwards GC. The validity of similarity theory in the roughness sublayer above forest. *Bound-Lay Meteorol* 1998;87:69–99.
- [37] Siqueira M, Lai CT, Katul G. Estimating scalar sources, sinks, and fluxes in a forest canopy using Lagrangian, Eulerian, and hybrid inverse models. *J Geophys Res* 2000;105:29,475–88.
- [38] Thomson DJ. Criteria for the selection of stochastic models of particle trajectories in turbulent flows. *J Fluid Mech* 1987;180:529–56.
- [39] Vermetten AWM, Ganzeveld L, Jeuken A, Hofschreuder P, Mohren GMJ. CO₂ uptake by a stand of Douglas-fir—flux measurements compared with model-calculations. *Agric Forest Meteorol* 1994;72:57–80.
- [40] Warland JS, Thurtell GW. A Lagrangian solution to the relationship between a distributed source and concentration profile. *Bound-Lay Meteorol* 2000;96:453–71.
- [41] Wilson NR, Shaw RH. A higher order closure model for canopy flow. *J Appl Meteorol* 1977;16:198–205.
- [42] Wofsy SC, Goulden ML, Munger JW, Fan SM, Bakwin PS, Daube BC, et al. Net exchange of CO₂ in a mid-latitude forest. *Science* 1993;260:1314–7.